

# Journal of Materials Chemistry B

Accepted Manuscript



This is an *Accepted Manuscript*, which has been through the Royal Society of Chemistry peer review process and has been accepted for publication.

*Accepted Manuscripts* are published online shortly after acceptance, before technical editing, formatting and proof reading. Using this free service, authors can make their results available to the community, in citable form, before we publish the edited article. We will replace this *Accepted Manuscript* with the edited and formatted *Advance Article* as soon as it is available.

You can find more information about *Accepted Manuscripts* in the [Information for Authors](#).

Please note that technical editing may introduce minor changes to the text and/or graphics, which may alter content. The journal's standard [Terms & Conditions](#) and the [Ethical guidelines](#) still apply. In no event shall the Royal Society of Chemistry be held responsible for any errors or omissions in this *Accepted Manuscript* or any consequences arising from the use of any information it contains.

**Novel bioactive nanocomposite cement formulations with potential properties:  
Incorporation of nanoparticle form of mesoporous bioactive glass to calcium  
phosphate cements**

**Ahmed El-Fiqi<sup>1,2</sup>, Joong-Hyun Kim<sup>1,2</sup>, Roman A. Perez<sup>1,2</sup>, Hae-Won Kim<sup>1,2,3,\*</sup>**

<sup>1</sup>Department of Nanobiomedical Science and BK21 PLUS NBM Global Research Center for Regenerative Medicine, Dankook University, Republic of Korea

<sup>2</sup>Institute of Tissue Regeneration Engineering (ITREN), Dankook University, Republic of Korea

<sup>3</sup>Department of Biomaterials Science, School of Dentistry, Dankook University, Republic of Korea

-----  
\* Corresponding author: Prof. H.-W. Kim

E-mail) kimhw@dku.edu; Tel) +82 41 550 3081; Fax) +82 41 550 3085

For: Journal of Materials Chemistry B

Injectable calcium phosphate cements (CPCs) with strong mechanical properties and improved biological performance have the potential to be extensively used for bone regeneration. Although many additive materials have been incorporated to CPCs in order to achieve improvements in their mechanical and biological properties, somehow the results have not been fully satisfactory. Here we focus on using nanoparticle form of mesoporous bioactive glass (mBGn) as additive nano-components for alpha-tricalcium phosphate-based CPCs. The effects of incorporating mBGn at up to 10 wt% into the CPCs were examined in depth with respect to the setting time, morphology, injectability, wash-out properties, consistency, ionic release, pH change, and mechanical strength. The addition of mBGn significantly increased the surface area (for both the as-cemented and the hydrated compositions) and also significantly accelerated the setting reaction of the CPCs. The injectability and the anti-washout property of the CPCs were remarkably enhanced with the addition of mBGn. In striking contrast to the case of pure CPCs, the morphological changes observed in simulated body fluid (SBF) revealed a spherical development of apatite crystals, replicating the nanospherical morphology of the mBGn and consequently resulting in nano-micro-roughened surface. The mechanical compressive strength substantially increased after SBF immersion and significantly higher values were recorded for mBGn/CPC as compared to pure CPCs. The ion release, including that of calcium, phosphate, and silicon, was recorded at substantial levels during the test period, and the addition of mBGn caused changes in the pH towards less acidic. The in vivo study of the mBGn/CPCs in rat subcutaneous tissue confirmed excellent tissue compatibility with little evidence of inflammatory reactions while exhibiting viable fibroblastic cells with a substantial presence of mature endothelial cells surrounding the cements. When implanted in a rat calvarium defect, a substantial degradation of the samples was noticed at the interfacial region. The proposed mBGn/CPC is a novel, promising cement formulation for the repair and regeneration of bone due to setting characteristics, physico-chemical and mechanical properties, and excellent in vivo tissue compatibility and bioactivity.

**Keywords:** calcium phosphate cements, mesoporous bioactive glass; nanoparticles; setting reaction; surface area; ionic release; bioactivity; mechanical properties; bone regeneration

## 1. Introduction

Calcium phosphate cements (CPCs) have found widespread uses in the repair and regeneration of bone tissues.<sup>1-3</sup> Particularly, the self-setting properties of the CPCs allow for potential utility as unique injectable inorganic biomaterials, which ultimately enables surgical treatments customized to the shape of the targeted defects.<sup>4-6</sup> Different compositions of calcium phosphate-based powders that can harden when mixed with water-based liquid have been discovered, including a mixture of tetracalcium phosphate (TTCP) and dicalcium phosphate anhydrous (DCPA), alpha-tricalcium phosphate ( $\alpha$ -TCP), and  $\beta$ -TCP/monocalcium phosphate monohydrate (MCPM).<sup>7-8</sup> Among these,  $\alpha$ -TCP, which is set by the phase transformation into calcium-deficient hydroxyapatite (CDHA), has been widely researched.<sup>9-13</sup> The final cement product, CDHA, is the primary inorganic component of extracellular matrix (ECM) of bone and thus provides a high level of biocompatibility and osteoconductivity.<sup>14</sup>

However, the crystalline CDHA phase has a very low degradation rate *in vivo* and is extremely brittle, restricting its potential use to non-load bearing parts.<sup>15-19</sup> Many studies have shown CPCs to enable osteogenic differentiation of osteoblasts and stem / progenitor cells *in vitro* as well as to have good tissue compatibility and bone formation *in vivo*.<sup>8, 12, 20-25</sup> Nevertheless, some properties, such as the degradability and mechanical strength, need to be significantly improved.<sup>15-19</sup> Moreover, substantial effort has been exerted to improve the osteogenic properties of the CPCs and to endow them with therapeutic efficacy in order to stimulate cellular actions for rapid healing and regeneration.<sup>6, 21, 26-28</sup>

While the properties of the CPCs can be possibly controlled in part by fine-tuning the powder composition, some significant changes can be made by using a composite approach. Many additive materials have been introduced to improve the properties of CPCs.<sup>20-21, 29-40</sup> Polymeric materials, including natural polymers in solution forms (chitosan, gelatin, collagen, and alginate) or synthetic polymers in particulate forms, e.g. poly (lactic-co-glycolic acid) (PLGA), have been widely used to primarily improve the ductility of the brittle cements.<sup>18-19, 40-49</sup> Furthermore, nanomaterials, such as carbon nanotubes and nanofibers, have also been incorporated and have shown to improve the physico-chemical and mechanical properties.<sup>21, 31, 33-34, 37, 50-51</sup> The incorporation of bioactive

nanomaterials into CPCs is considered to be an intriguing and promising method that can significantly alter the physico-chemical, mechanical, and biological properties. However, a very limited class of inorganic nanomaterials can be acceptable, i.e., these have to be biocompatible and must improve the properties while preserving the self-hardening character of the CPCs.

Here, we focus on the nanoparticulate form of mesoporous bioactive glasses (mBGn) as a novel inorganic additive for CPCs. Indeed, bioactive glass nanoparticles (BGn) have recently gained great attention as promising nano-bioactive materials, particularly targeting hard tissues.<sup>52–56</sup> The physico-chemical and bioactive properties associated with their nanoscale and high surface area are extraordinary when compared to the conventional microparticulate form of BG.<sup>57</sup> Some recent studies have shown that the incorporation of BGn into biopolymeric materials significantly improved the mechanical and biological properties.<sup>58–59</sup> Moreover, the BGn used to fill small defects in tooth structures have shown excellent dentin re-mineralization ability.<sup>60</sup>

On the other hand, the mesoporous form provides unique physico-chemical properties to BG materials.<sup>61,82–83</sup> The mesoporous form of BG (mBG), first reported by Yan *et al.*<sup>84</sup>, has been developed to have a highly ordered mesopore structure with pore sizes ranging from a few to tens of nanometers. The bioactivity and degradation behaviors of the mBG could be significantly enhanced with respect to non-mesoporous BG, due to the increased specific surface area and large pore volume.<sup>85–88</sup> Furthermore, the presence of mesopores allows for effective loading of growth factors and drugs<sup>82,93,89,90</sup>. While the mBG have been formulated in different shapes including micro-granules, fibers and scaffolds<sup>91,92</sup>, the nanoparticle form has recently been developed, holding great promise for use as nano-additives and nano-carriers<sup>61,82–83</sup>

Therefore, the incorporation of mBGn to CPCs is considered to achieve both merits of mesoporosity and nanoscale dimension of the additives within CPC composition. In fact, some recent studies have incorporated the microparticulate forms of BG into CPCs in order to utilize the BG-driven bone-bioactivity.<sup>20,36</sup> In contrast to these previous works, the current study was the first to utilize the nanocomponent of BG as the additive to CPCs, namely, a nanocomposite approach. From preliminary tests, we have noticed that the addition of mBGn induced substantial improvements in some of the properties of CPCs, signifying the potential development of mBGn-added nanocomposite cements as

bone injectables. Therefore, in the current study we systematically report the influence of mBGn addition on the physico-chemical and mechanical properties of CPCs, including their setting reaction, injectability, wash-out resistance, consistency, ionic release, pH change, and compressive strength. Furthermore, the *in vivo* tissue biocompatibility of the nanocomposite cements was addressed to confirm the feasibility for bone repair materials. This report will highlight the intriguing and remarkable effects of the mBGn-addition to CPC, and may spur further developments of a new class of nanocomposite injectable bone cements.

## 2. Results

### 2.1. Cement powders

A newly developed sono-assisted sol-gel method was used to prepare the mBGn powder.<sup>61</sup> Nano-sized particles with well-developed spherical morphology and mesoporous structure were effectively produced by applying ultra-sound and using PEG as a structure-directing agent under alkaline conditions. TEM images of the as-prepared mBGn revealed nanospheres of about 80 nm in size and with worm-like mesopores (~5 nm) (**Fig. 1a**). TEM-EDS analysis confirmed an elemental composition equivalent to the designed nominal glass batch (Si/Ca = 75:25). The in vitro bone-bioactivity of the mBGn assayed through the SBF immersion test revealed that poorly-crystallized apatite peaks were developed and that the intensities in XRD patterns increased with immersion time (**Fig. 1b**).

The physical properties of the mBGn and  $\alpha$ -TCP powders that were used to fabricate the CPC/mBGn formulations, such as the particle size, surface area, and  $\zeta$ -potential, are summarized in **Table 1**. Compared to  $\alpha$ -TCP, mBGn had a significantly higher specific surface area (~6 times). The mBGn had clear mesoporous properties, with a pore volume of 0.133 cm<sup>3</sup>/g and a pore size of 4.9 nm. The  $\zeta$ -potential of mBGn was more negative than that of  $\alpha$ -TCP (-29 mV vs. -15 mV).

### 2.2. Cement setting and morphology

The cement powders were formulated with varying mBGn contents (up to 10%) in  $\alpha$ -TCP, and the mixtures were hardened after mixing with a liquid at varying ratios. The morphology, phase, and chemical structure of the as-hardened cement samples were characterized, and the SEM images of the composite powders revealed the existence of ultrafine nanoparticulate mBGn surrounding the  $\alpha$ -TCP micron-sized powders (**Fig. 2a**). The XRD patterns confirmed a main  $\alpha$ -TCP phase (JCPDS Card No. 09-348) for all prepared cement samples (**Fig. 2b**). Very weak peaks corresponding to traces of  $\beta$ -TCP (JCPDS Card No. 09-169) and HA (JCPDS Card No. 09-432) were also labeled. ATR FT-IR spectra showed phosphate-related bands at around 559, 597, and 1020 cm<sup>-1</sup> and silicate-related bands at around 476, 797, and 1220 cm<sup>-1</sup> (**Fig. 2c**). The silicate-related bands increased in intensity as the mBGn content increased.

The Gilmore needle method was used to measure the setting time of the cements with

different L/P ratios (0.55, 0.65, and 0.75 ml/g).<sup>62</sup> An increase in the L/P ratio resulted in an increase of the setting time. Of note, the addition of mBGn progressively decreased the setting time from 108 min (0% mBGn) to 25 min (10% mBGn) at an L/P ratio of 0.55 ml/g.

The as-hardened cements were soaked in SBF for 7 days in order to investigate the changes in morphology and phase.<sup>53, 55, 61</sup> The SBF-soaked samples showed obvious morphological changes as compared to those before soaking (**Fig. 4a–d**). While pure CPCs showed ruffled apatite crystallites that were typical of  $\alpha$ -TCP-based CPCs, the 10% mBGn cement revealed a microspherical development that upon closer examination presented a nanotopology similar to that of pure CPC. The XRD spectra showed the development of the characteristic hydroxyapatite diffraction patterns (JCPDS Card No. 09-432) as shown in **Fig. 4e**, and the apatite peak intensities of the 10% mBGn cement appeared to be stronger than those of pure CPC. A substantial change in the phosphate bands (intensity increase at 561, 601 and 1023  $\text{cm}^{-1}$ ) was also related to the change of the  $\alpha$ -TCP to HA (**Fig. 4f**).

### 2.3. Surface area and porosity

The specific surface area and the porosity of the cements with varying contents of mBGn before and after immersion in SBF were evaluated with respect to BET and Hg intrusion measurements. An increase in mBGn resulted in a significant increase in surface area both before and after SBF soaking (**Fig. 5a**). Before SBF immersion, the 0% mBGn and 10% mBGn cements showed a surface area of about 3.5  $\text{m}^2/\text{g}$  and 14.2  $\text{m}^2/\text{g}$ , respectively. After immersion the values increased significantly to 21.6  $\text{m}^2/\text{g}$  for 0% mBGn and 31.7  $\text{m}^2/\text{g}$  for 10% mBGn.

Furthermore, the porosity of the cements before the SBF-soaking increased only slightly with an increase in the mBGn content while the samples had similar porosity levels after SBF-soaking (**Fig. 5b**). Compared to the change in the surface area, the porosity change was very small.

### 2.4. Compressive strength

The mechanical performance of the cement samples under compression was also tested before and after SBF treatment (**Fig. 6**). Before SBF-soaking, the samples (as-hardened & not transformed to HA) showed very low compressive strength with a small increase in mBGn additions from 0.87 MPa (0%

mBGn) to 1.84 MPa (10% mBGn). Immersion in SBF significantly improved the strength of all the cements, and the increase in the mBGn addition gradually increased the strength value to 12 MPa for pure cement to 26 MPa for 10% mBGn cement.

### 2.5. Injectability, anti-washout, and consistency

The successful utilization of cements in clinical applications requires for cement formulations with good injectability<sup>5</sup>. Herein, we have examined the injectability of the CPC pastes with various mBGn contents by using a syringe injection set-up fitted in a uniaxial compression machine. The injectability percentage was obtained from the amounts of CPC pastes extruded from the syringe under a maximum applied force of 150 N, and the representative injectability curves of the CPC pastes incorporating 0, 5, and 10% mBGn obtained under a compression speed of 15 mm/min were presented (**Fig. 7a–c**). The curves were used to calculate the injectability percentage (**Fig. 7d**), which showed initial improvements by increasing the mBGn contents to up to 5%. The injectability increased from 60% for pure cement to 75% for the 5% mBGn-added cement, and then showed a slight decrease to 71% for the 10% mBGn-added cement, which was nevertheless still higher than that of pure CPC.

The resistance to wash-out in aqueous environments can be considered to be an indicator of the degree of cement cohesion. The wash-out resistance of the as-prepared CPC/mBGn samples was tested in PBS solution through mechanical shaking, and the amount of washed-out particles was determined at the end of the test. The pure CPCs showed around a 95% disintegration, whereas a significant decrease in wash-out (~12%) was observed upon adding 10% mBGn (**Fig. 8a**).

The consistency is another factor that affects the handling properties of the CPC/mBGn pastes, and it was evaluated from measurements of the spread diameters of the cement pastes after applying an external load. A spread diameter of 8.8 cm was recorded for a pure CPC paste, indicating a liquid-like paste. However, after adding mBGn, the spread diameter decreased considerably (~5.3 cm for 2% mBGn, 2.8 cm for 5% mBGn and 2 cm for 10% mBGn), showing that the mBGn had an effective role in controlling the consistency of the paste.

## 2.6. Change in ionic concentration and pH

We examined the change in the ion concentrations of the medium since the ionic dissolution and re-precipitation processes are accompanied with cementation and phase transformation of the CPC-based cements. Si ions, along with Ca and P ions, were recorded via ICP-AES analysis<sup>69-72</sup>. First, the ionic change of the mBGn showed an initial rapid Ca and Si ion release within the first day of immersion, followed by a continual increase in Ca release while the Si ions were very slowly released (**Fig. 9a**). Next, the ionic change of the cements was examined. The 0% mBGn cements exhibited an initial rapid increase of Ca and P ions that was then followed by a rapid drop afterwards (**Fig. 9b**). The 10% mBGn cements showed an almost similar Ca and P ion release behavior as that of the 0% mBGn cement, while the Si ions continued to be released (**Fig. 9c**)

The changes in the pH during the immersion of the cements in a PBS solution at a pH of 7.4 were monitored (**Fig. 10**). For all cases, the pH initially increased (within a day) and then decreased over time. However, the incorporation of the mBGn shifted the pH change towards less acidic. After 4 weeks, the pH changed down to around 5.9 for the 0% mBGn whilst it was around 6.6 for the 10% mBGn.

## 2.7. Protein adsorption capacity

The protein adsorption capacity of the cements was examined after immersion in SBF (**Fig. 11**). Cytochrome C (Cyto.c) was used as a model protein, and the concentrations used ranged from 0.125 to 4 mg/ml. The adsorbed protein content increased with an increase in the Cyto.c content for all cement groups. In particular, an increase in the mBGn content significantly increased the Cyto.c adsorption content.

## 2.8. In vivo biocompatibility

The histological evaluations of the subcutaneous rat tissues revealed that both the implanted 0% and 10% mBGn cements were biocompatible at 4 weeks after surgery (**Fig 12**). All samples showed good biocompatibility, and the two groups had no differences in their histological features. The samples were encapsulated by very thin granulation tissues with minimal inflammatory signs, and proper neovascularization was observed around the samples.

The histological H&E images of the cements implanted in the rat calvarial bone defects were also assessed at low and high magnifications (**Fig. 13**). Six weeks after implantation, substantial levels of new bone formation were detected for both the 0% and 10% mBGn cements. The new bone was formed mainly from the defect margins of the host bone or the dura matter surface, which extended towards the surface of the samples in block form. Upon closer examination of the interface of the sample/tissue, new bone ingrowth into the material was notable for the 10% mBGn cement, making the interface more intermixed or complicated. The notable difference between the two groups was in their degradation. As compared to the 10% mBGn cements block, a degradation of the 0% mBGn cements block was not remarkable. For the 0% mBGn cements, the new bone formed mostly on the surface of the samples. However, a marked bone invasion into the scaffold was observed for the 10% mBGn cement, which was in accordance with the degradation sign of the cement at the interfacial regions.

### 3. Discussion

Here we proposed novel  $\alpha$ -TCP-based cement formulations incorporated with bioactive nano-component, mBGn. In fact, many studies have reported on the incorporation of polymeric additives to CPCs in order to improve their mechanical and/or biological properties.<sup>15, 19, 21, 31, 38, 41-49</sup> However, very few studies have utilized inorganic nanoparticles<sup>30, 32, 35, 40</sup> and in particular, mBGn, which have been recently recognized for the excellent bone like-apatite bioactivity and even for their drug delivery capacity.<sup>53, 55, 59, 61, 82-83</sup> Sizes of less than a hundred nanometers potentiate the surface-related properties, such as the surface reactivity, molecular interactions, and ionic release. Furthermore, a level of degradability and nontoxic dissolved products allow for fascinating nanomaterial platforms that are potentially useful for tissue regeneration. The high level of mesoporosity provides an additional loading and delivery ability of the therapeutic proteins and drugs to the nanomaterials.

Small additions of mBGn significantly changed the physico-chemical properties of the nanocomposite cements. First, the setting reaction was notably accelerated, and the ultrafine glassy nanoparticles can be deduced to possibly have some role in the hardening reaction of the  $\alpha$ -TCP powder, i.e., the dissolution-reprecipitation processes with the possible involvement of the Ca ions released from the

mBGn (as revealed in the ionic release test) of the hardening process. Actually, the acceleration of setting and hardening can also be correlated to an increased rate of hydroxyapatite formation due to mBGn addition, as witnessed from the results. Another possible explanation can be attributed to the fact that the mBGn, with its mesoporous properties, may absorb and/or adsorb some free (extra) water from the liquid phase, which can result in a decrease in the starting L/P ratio of the CPCs, and hence indirectly reduce the setting time. Interestingly, after SBF immersion, the mBGn-incorporated cements revealed the formation of an apatite crystal morphology with microspherical islands, reflecting the possible crystal growth mechanism of the initial nanospheres, and this was in contrast to what happened with pure CPCs. In both cases, the final cementation products were apatite, with nano-roughened morphologies being similar, i.e., nano-plated flowering of the crystallites.

One notable difference of the nanocomposite cements from pure CPC is the surface area, which was consistently recorded for both SBF-immersed and non-immersed samples. The mBGn-added cements had a significantly higher surface area than that of pure cement, and this was primarily due to the presence of ultrafine nanoparticles with their high surface area. The surface area of pure mBGn was an order of magnitude higher than that of pure  $\alpha$ -TCP particles ( $54 \text{ m}^2/\text{g}$  vs.  $0.86 \text{ m}^2/\text{g}$ ). Therefore, even small additions (up to 10%) of the mBGn significantly increase the surface area of the cement formulations. After being changed into an apatite phase in SBF medium, both the cement groups had a significantly increased surface area, due to the nanocrystalline morphology of the developed apatite and the mBGn-incorporated cement still showing a higher surface area resulting from the growth of microspherical apatite islands from the mBGn. An important outcome of this enhanced surface area has been observed to result in an increase in the protein adsorption, as revealed in the adsorption test using Cyt c as the model protein. Although more in-depth work may be needed, this protein adsorption result supports the potential use of mBGn-added nanocomposite cements for protein loading and delivery. Furthermore, the cellular response to the cements, which generally affected by the adhesive protein adsorption events<sup>74-77</sup> can also be positively considered, though this is yet to be studied in the future.

In addition to the setting reaction and surface reactivity, the compressive mechanical strength was also significantly improved by the incorporation of mBGn, particularly after soaking in SBF. The strength of 10% mBGn/CPC was more than twice as high as that of pure CPC (26 MPa vs. 12 MPa). The increase in strength can be attributed to the nanocomposite effects, i.e., the nanoparticles dispersed in the cement

matrix could exert size-related reinforcement effects.<sup>30, 32, 35, 40</sup> Moreover, the bioactive nano-components are expected to be well integrated with the cement matrix during the transformation of the  $\alpha$ -TCP and mBGn into HA in SBF through the entanglement of apatite nanocrystals. Although here we observed the mBGn addition significantly improved the strength of CPCs during the SBF-immersion, the information on the strengthening effects of mBGn in the real *in vivo* conditions might be rather limited; presumably due to the relatively short test period (7 days), which not reflecting the time-dependent degradation behaviors of the cements and the consequent change in mechanical strength. Therefore, the mechanical tests of cement samples with long-term periods in SBF are considered to require in the future.

The injectability, wash-out resistance, and consistency are of special importance for practical applications of cements, particularly when used in an injectable form in a wet condition. The presence of ultrafine glassy nanospheres within the CPC paste enhanced the flow and tuned the rheology, as observed from the injectability measurements. The mBGn incorporation improved the injectability (60% for 0% mBGn, 75% for 5% mBGn, and 71% for 10% mBGn). Actually, the particle size and the shape of the cement powder are expected to have an effect on the injectability. Namely, powders with smaller sizes and a spherical shape may contribute to good injectability.<sup>30, 78-79</sup> The spherical powder itself is easy to flow, and thus, a paste has good handling properties and injectability when it is prepared using a spherical powder.<sup>66</sup> The resistance to wash-out was also significantly improved with the addition of mBGn. While the as-cemented pure CPC samples were easily washed out and the initial shape and mass was not preserved, those containing 5% and 10% mBGn were preserved almost completely in their initial status, demonstrating that the nanocomposite cement components possessed a high cohesive force and resisted the disintegration of particles caused by exposure to water molecules.

Cement pastes with tunable consistency can provide a range of applicability for defects of various shapes. The consistency test showed considerable variations in the paste consistency as the amount of mBGn added changed. Hence, the consistency can be tuned in accordance with the amount of mBGn, such as less viscous, fluid-like, or flows quickly, otherwise thick, putty-like, or flow moderately. These noticeably-improved properties in the nanocomposite cements, including the improved injectability, anti-wash-out, and consistency, indicate that the novel cement formulations have potential for practical applications as injectable bone repair materials.

The study of the ionic release of the cements clearly showed the type and dose of ions that might affect the biological response. While pure CPC released Ca and P ions, the mBGn-added cements additionally released Si ions, yet the Ca and P ions that were released were comparable for both groups. Notably, the Ca and P ion release decreased after peaking at day 1, which indicates that the Ca and P precipitate again. Furthermore, while the Ca ion released from the bare mBGn was substantial, the 10% mBGn-added cement released Ca ions at a level similar to that of the 0% mBGn cement, indicating that the Ca ions released from the 10% mBGn should also be involved in the re-precipitation process, and this again suggests that there is more rapid mineralization of the mBGn-added cements. This ionic release result also supports the increased setting reaction of the mBGn-added cements, i.e., the released ions play a role in accelerating the re-precipitation process, and thus in hardening and apatite formation. In addition to the Ca and P ions, the Si ions were recorded at high levels in the mBGn-added cements during the study period, which suggests that Si might not be primarily involved in the precipitation process. Rather, the Si ions are largely present in the release medium, and this fact would contribute to the possible role that the Si ions played in the biological reactions, such as in cell proliferation and osteogenic differentiation, since Si ions have been indicated to be a stimulator of those processes for bone-related cells.<sup>69-73</sup>

The different ionic levels also influenced the change in the pH of the cements. The incorporation of the mBGn altered the pH to become less acidic. While pure CPCs changed the pH down to ~6.0 after 4 weeks, the 10% mBGn cement showed a pH of ~6.6 at the same time period. The change in the pH should be closely related to the ionic release and to the re-precipitation. The additional Ca ions released from the mBGn in the nanocomposite cements may result in an increased pH. Based on the changes in the pH, we can thus surmise the possible biological effects that benefited from the mBGn-added cements, such as maintaining a pH in a more neutral state and thus favoring cellular viability. However, the in vivo conditions are quite open, under a dynamic flow, and thus the local drop in the pH will be buffered rather easily. Therefore, a situation is also possible that might negate the pH difference that was observed in this in vitro study. The changes in the observed pH are nevertheless not a negative aspect of the cements that were developed.

We directly assessed the in vivo biocompatibility of the nanocomposite cements without performing in vitro cell tests since the in vivo test is considered to provide more clear-cut information.

First, the cement samples were subcutaneously implanted and showed excellent tissue response, including no significant inflammatory signs, abundant proliferative cellular engraftment, and substantial angiogenesis with endothelial cells. No significant histological differences were noted between the cements with and without mBGn, implying that the mBGn-added cements provided excellent biocompatibility, like pure CPCs. Further experiments in calvarium defects also presented good tissue reactions, particularly in the formation of neo-bone tissues surrounding and at the interface areas of the cements. Noticeably, the mBGn-added cements exhibited more signs of degradation in the materials, with the replacement of bone forming cells and neo-bone tissue. The mBGn cement/tissue interface changed more substantially than that for pure CPC/tissue. This calvarium result indicates another positive aspect of the nanocomposite cements since the apatitic CPCs have been considered to have very limited degradability and thus much effort has been devoted to improve their degradability.<sup>15–20, 36, 38, 80–81</sup> Although more studies will be needed to fully characterize the in vivo degradation of these cements with longer implantation periods and with injectable forms, the present in vivo findings suggest that this novel cement formulation has enhanced degradability.

#### 4. Conclusions

A novel cement formulation based on CPCs was developed by the nanocomposite approach using mesoporous bioactive glass nanoparticles (mBGn). The mBGn with a nanospherical shape, high mesoporosity, and bone-like apatite bioactivity were added up to 10 wt% and significantly altered the physico-chemical, mechanical, and biological properties of the CPCs. The mBGn-added cements possessed a substantially improved surface area, enabling a higher protein adsorption. The setting reaction was significantly enhanced by the addition of the mBGn, and the microstructure that developed for the nanocomposite cements revealed spherical island morphology, comprised of a number of apatite nanocrystallites. The compressive strength of the cements was significantly improved by the addition of mBGn, and the pH changed towards less acidic in the nanocomposite cements. The Ca and P ionic release-precipitation behaviors were comparable for both the pure and the mBGn-added cements, and the mBGn-cement had additional Si ion release. The mBGn addition

considerably improved the injectability, anti-washout, and consistency of the cements, potentiating their practical use as injectable bone substitutes. The in vivo observation in subcutaneous tissue confirmed the tissue compatibility of the proposed nanocomposite cements. Furthermore, the in vivo study in bone defects revealed a more rapid degradation sign of the cements in concert with the replacement by neo-formed bone tissue. The present results demonstrated that mBGn can have an effective role as novel nano-components that can improve the physico-chemical, mechanical, and biological properties of CPCs, and these findings support their potential use as bone-regenerative injectables.

## 5. Experimental

### 5.1. Materials

Tetraethyl orthosilicate (TEOS,  $C_8H_{20}O_4Si$ , 98%), calcium nitrate tetrahydrate [ $Ca(NO_3)_2 \cdot 4H_2O$ , 99%], calcium carbonate ( $CaCO_3$ ,  $\geq 99.0\%$ ), calcium hydrogen phosphate ( $CaHPO_4$ , 98.0–105.0%), disodium hydrogen phosphate ( $Na_2HPO_4$ ,  $\geq 99.0$ ), poly(ethylene glycol), [PEG,  $(C_2H_4)_nH_2O$ ,  $M_n = 10000$ ], ammonium hydroxide ( $NH_4OH$ , 28.0%  $NH_3$  in water,  $\geq 99.99\%$  metal basis), methanol anhydrous ( $CH_3OH$ , 99.8%), high purity chemicals for SBF solution, tris hydroxymethyl aminomethane, 1N hydrochloric acid (1N HCl), and phosphate buffered saline (PBS) tablets were all purchased from Sigma-Aldrich and were used as-received without any further purification. Ultra-pure deionized water (18.2 M $\Omega$ .cm, Millipore Direct-Q system) was used throughout the experiments.

### 5.2. Synthesis of mBGn

Mesoporous bioactive glass nanospheres with a well-developed spherical morphology and mesoporous structure were prepared under alkaline conditions using an ultra-sound assisted sol-gel method with PEG as a template.<sup>61</sup> A nominal composition of 85%  $SiO_2$  and 15%  $CaO$  in mol was used for the glass preparation. In a typical synthesis, 5 g of PEG were dissolved in 120 ml absolute methanol via magnetic stirring, and then the pH of the solution was adjusted to 12.5 by adding  $NH_4OH$ . Next, 0.179 g of  $Ca(NO_3)_2 \cdot 4H_2O$  were dissolved in the previous solution via magnetic stirring. In another vessel, 0.895 g TEOS was diluted with 30 ml absolute methanol and was then added drop-

wise to the pH-adjusted solution while vigorously stirring and simultaneously applying high power ultra-sound for 20 min (10 seconds on/10 seconds off). After 24 hours of vigorous magnetic stirring, a white precipitate was separated and washed with water/ethanol in 3 centrifugation/redispersion cycles at 5000 rpm for 5 min and was then dried at 70 °C overnight. To remove the PEG template, the dried powder was heated to 600 °C at a heating rate of 1 °C/min and was finally calcined at 600 °C for 5 hours in air and was then stored under vacuum for further use.

### 5.3. Synthesis of $\alpha$ -TCP and cement formulations

$\alpha$ -Tricalcium phosphate [ $\alpha$ -TCP,  $\alpha$ -  $\text{Ca}_3(\text{PO}_4)_2$ ] powder was prepared from a mixture of  $\text{CaHPO}_4$  and  $\text{CaCO}_3$  by sintering at 1400 °C for 2 hours with subsequent rapid quenching in air. The obtained  $\alpha$ -TCP was milled in a planetary ball mill (Retsch, PM 100 CM, Germany) and then sieved and mixed with 2 wt% hydroxyapatite powder (Alfa Aesar, Karlsruhe, Germany; sintered at 900 °C for 3 hours). Calcium phosphate cement (CPC) pastes incorporated with 0, 2, 5 and 10 wt% of mBGn (by replacing CPC powder proportions with the equivalent amounts of mBGn powder) were prepared at a liquid to powder (L/P) ratio of 0.65 ml g<sup>-1</sup> using a 2.5 wt% aqueous solution of  $\text{Na}_2\text{HPO}_4$  as a liquid. The  $\alpha$ -TCP and mBGn powders were mixed well using a vortex mixer for 5 min, and then the liquid was added to the nanocomposite powder, and the mixture was quickly homogenized to form the CPC/mBGn nanocomposite paste. The paste was introduced into Teflon moulds and was finally left for setting. Finally, the samples were immersed in SBF for 7 days to complete the transformation of  $\alpha$ -TCP into calcium-deficient hydroxyapatite (CDHA).

### 5.4. Characterization of physicochemical properties

The phases of the mBGn,  $\alpha$ -TCP, and cement samples were analyzed via powder X-ray diffraction (XRD, Rigaku, Ultima IV, Japan) before and after immersion in SBF. X-rays were generated using Cu K $\alpha$  radiation ( $\lambda = 1.5418\text{\AA}$ ) at 40 mA and 40 kV, and the data were obtained at diffraction angles ( $2\theta$ ) from 4° to 70° with a step size of 0.02° and a scanning speed of 2°/min. The specific surface area, pore volume, and pore size of the prepared mBGn and the specific surface area of the CPC/mBGn composite cements were obtained from the  $\text{N}_2$  adsorption-desorption measurements.  $\text{N}_2$  adsorption-desorption isotherms were obtained at -196.15 °C on an automated surface area and pore size analyzer (Quadrasorb SI, Quantachrom instruments Ltd., USA.). The samples were degassed under

vacuum at 300° C for 12 h prior to analysis, and the specific surface area was calculated according to the Brunauer-Emmett-Teller (BET) method. The pore size distribution of the mBGn was determined using the N<sub>2</sub> desorption branch of the obtained N<sub>2</sub> adsorption-desorption isotherms on the basis of non-local density functional theory (NLDFT).

The attenuated total reflectance - Fourier transform infrared spectra (ATR-FTIR) of the mBGn and cement samples were obtained before and after SBF immersion with a resolution of 4 cm<sup>-1</sup> on a Fourier-Transform infrared spectrometer (FT-IR, Varian 640-IR, Australia) at a range 4000–400 cm<sup>-1</sup> using the GladiATR diamond crystal accessory (PIKE Technologies, USA). The particle size distribution of the milled  $\alpha$ -TCP powder was obtained using a laser particle size analyzer (Mastersizer 2000, Malvern Instruments, UK). The surface charge of the mBGn and of the  $\alpha$ -TCP powders were investigated via zeta ( $\xi$ ) surface potential measurements using a Laser Doppler electrophoresis (LDE) instrument (Zetasizer Nano ZS, Malvern Instruments, UK). The zeta-potential was measured in water (25° C) at a pH of 7 with an applied field strength of 20 V/cm. Five measurements were taken with each measurement being the average of 40 subruns.

### 5.5. Setting time measurement

The setting times for the CPC/mBGn composite pastes were determined according to the ASTM-C266-08 standard at different L/P ratios of 0.55, 0.65, and 0.75 ml g<sup>-1</sup> using a Gillmore needle.<sup>62</sup> The setting time was considered to be the time interval it takes from when the powders are mixed with the liquid to the time when a needle 2.13 mm in diameter and 113.4 g in weight could be loaded on the surface of the cement paste without making any visible imprint. The measurement was taken for three independent samples for each cement formulation.

### 5.6. Electron microscopy observations

The mesoporous structure, particle size and composition of the prepared mBGn were observed via high-resolution transmission electron microscopy (HR-TEM, JEM-3010, JEOL, Japan) equipped with energy dispersive X-ray spectrometry (TEM-EDX, Oxford Instruments). The surface morphology of the CPC/mBGn composite cements was observed through high resolution scanning electron microscopy (SEM, JSM-6510, JEOL Japan) equipped with SEM-EDX (INCA x-act, 51-ADD0076, Oxford Instruments). Before the SEM observations, the cement samples were sputter-coated with

platinum for 120 s using an automatic magnetron sputter coater (Cressington 108 Auto sputter coater, UK).

### 5.7. Porosity measurement

The porosity of the CPC/mBGn samples was measured via mercury intrusion porosimetry by using an automatic mercury intrusion porosimeter (PoreMaster<sup>®</sup>, Quantachrom instruments Ltd., USA). Three accurately weighed cement disks (6 mm diameter, 3 mm height) from each CPC/mBGn formulations were inserted in the analysis tube. The samples were analyzed at low and high pressures, and each measurement was performed in triplicate.

### 5.8. Compressive strength test

The mechanical strength of the cements was evaluated through a compressive mechanical test using a universal testing machine (Instron 5966, USA) with a 10KN load cell under a cross-head speed of 1 mm/min. A set of cylindrical specimens (6 mm in diameter and 12 mm in height) of each composition were formulated by transferring the cement paste to a cylindrical Teflon<sup>®</sup> mold. The tested specimens were obtained from two different groups: one group had been immersed in SBF for 7 days at 37 °C (SBF-immersed) and the other had not (non-immersed). The test was performed on wet samples, at least 6 samples were tested for each composition, and the average values  $\pm$  the standard deviation were reported.

### 5.9. Ion release analysis

Calcium, phosphorus, and silicon ion release were measured from bare mBGn and from CPC samples incorporating 10 wt% mBGn at 37 °C for up to 14 days. The CPC disks (0.450 g in weight, 15 mm in diameter, and 2 mm in thickness) and the 20 mg mBGn samples were immersed in 10 ml of deionized water buffered at a pH of 7.4 with Tris-HCl buffer and were then incubated at 37 °C without refreshing the medium for different predetermined times. At the end of each duration, the release medium of each sample was withdrawn and centrifuged at 15000 rpm for 15 minutes, and the clear supernatants were collected for ion determination through inductively coupled plasma atomic emission spectrometry (ICP-AES; OPTIMA 4300 DV, Perkin-Elmer, USA). Three replicates of each sample were evaluated, and the average value was recorded.

### 5.10. pH change measurement

The changes in the pH produced during immersion of the CPC/mBGn samples in PBS were recorded using a bench-top pH-meter (Orion 3 STAR, Thermo electron, USA). For each CPC/mBGn formulation, three cement disks (6 mm diameter, 3 mm height) were immersed and incubated in a 10-ml PBS (pH 7.4) solution at 37 °C. The pH of the solution was measured at predetermined time points and the reported values are the mean  $\pm$  the S.D. collected from 3 independent samples.

### 5.11. Injectability test

The injectability of the cement pastes was measured through an extrusion test, as described elsewhere.<sup>63–64</sup> A certain amount of cement paste was introduced in a commercial syringe with a nozzle diameter of 2 mm (5 mL capacity and 14 mm inner diameter). The syringe was placed in an injection set-up fitted in a uniaxial testing machine (Instron 5966, USA). The test was performed at a constant injection speed of 15 mm min<sup>-1</sup>, and the extrusion was initiated 15 min after the cement powder was mixed with the liquid at an L/P = 0.45 ml g<sup>-1</sup> and was stopped when the applied force reached 150 N. The percentage of the injectability was calculated from the weight of the cement paste extruded from the syringe and the initial weight of the cement paste introduced into the syringe. Three specimens were tested for each formulation, and typical injectability curves were obtained by plotting the displacements of the syringe plunger versus the applied force.

### 5.12. Wash-out resistance test

The degree of the cohesion or the wash-out resistance of the CPC/mBGn cements was evaluated through mechanical shaking of the as-prepared samples in PBS solution. CPC disks (6 mm in diameter and 3 mm in thickness) were accurately weighed and were directly tested 2 hours after their preparation. The dry weight of each sample was recorded, and each sample was transferred to a 50-ml tube containing 50-ml PBS solution and was then placed in an incubator shaker (100 rpm) at 37 °C for 30 minutes. The samples were carefully taken out and were dried at 70 °C for 1 hour, and their weights were finally measured. The wash-out percentage was obtained by comparing the initial disk weight to the final disk weight after the wash-out test.

### 5.13. Consistency test

The consistency of the cement pastes was evaluated according to the method set forth in the ISO 1566 standard for dental zinc phosphate cement.<sup>65–68</sup> In this method, the consistency is defined as the diameter of the cement paste spread when a glass plate (140 ± 0.5 g) is placed on 0.5 ml of the paste 3 min after mixing. In the present study, a 145 g glass plates were placed on 0.5 ml samples of the cement pastes, and the spread diameters were measured after 3 min.

### 5.14. Protein adsorption study

The adsorption capacity of proteins onto the cement samples were evaluated by using Cyto.c as a model protein. The cyto.c adsorption onto CPC/mBGn cements before and after SBF immersion was obtained by soaking accurately weighed cement disks (6 mm diameter, 3 mm height) in solutions containing 0.125, 0.250, 0.50, 1, 2, and 4 mg/ml of Cyto.c. The amounts of Cyto.c adsorbed after 6 hours of immersion at 37 °C were determined via UV-Vis spectrometry (UV-Vis spectrometer, Libra S22, Biochrom, UK). A series of standard Cyto.c solutions in d-H<sub>2</sub>O were prepared, and their absorbance values were measured at  $\lambda_{\max} = 409$  nm. A linear calibration curve for Cyto.c was obtained at a concentration range of 0–125 µg/ml, which fits Lambert and Beers' law, which states  $A_{409} = 0.0071 C - 0.007$  ( $R^2_{\text{cyto.c}} = 0.9998$ ) where A is the absorbance at  $\lambda_{\max} = 409$  nm and C is the concentration in µg/ml.

### 5.15. In vivo implantation

Twelve-week-old male Sprague-Dawley rats were used for the experiments involving subcutaneous and calvarium implantations. The animals were individually housed under a controlled environment and were provided with standard pellet food and water *ad libitum*. All experimental procedures on animals were reviewed and approved in accordance to guidelines for animal care and use established by the Animal Care and Use Committee, Dankook University, Cheonan, South Korea.

The *in vivo* biocompatibility of the as-prepared pure CPC and mBGn-added CPC samples were assessed in the subcutaneous tissues of the rats. The animals were anaesthetized with an intramuscular injection of ketamine/xylazine. The skin on the dorsal region of the rat was shaved and disinfected with povidone iodine and 70% ethanol. A two-centimeter skin incision was made, and four small subcutaneous pockets were made on the back, laterally from the spine, by blunt dissection.

Four as-prepared samples of 0% and 10% mBGn-added CPC discs (6 mm diameter and 3 mm height) were rinsed with 70% ethanol/PBS solutions and were then sterilized using the ethylene oxide gas (EO gas) sterilization method. The sterilized samples were implanted into the prepared pockets, and then the incision was sutured using a monofilament suture. The animals were sacrificed 2 weeks after surgery, and then samples were harvested for histological analysis.

The *in vivo* bone formation was evaluated by implanting the as-prepared 0% and 10% mBGn-added CPC discs (6 mm diameter and 3 mm height) in a critical-sized rat calvarial bone defect model. The cement samples were sterilized as described above. Under the anesthesia conditions mentioned above, the hair over the skin on the dorsal region of the cranium was shaved, and the region was aseptically prepared for surgery using povidone and 70% ethanol. A linear mid-line skin incision was made over the calvarium, and a full-thickness flap of the skin and periosteum was elevated. Two full-thickness calvarial bone defects with 6-mm diameter were created in each rat using an electric trephine. The samples were implanted into each calvarial defect, and the animals were randomly allocated into 0% and 10% mBGn-added groups. Then, the subcutaneous tissue was closed with absorbable materials, and skin incisions were sutured with non-absorbable materials. The animals were sacrificed 6 weeks after implantation to collect the calvaria, and the specimens were harvested immediately after sacrifice and were fixed in 10% neutral buffered formalin for 24 hours at room temperature.

#### **5.16. Histological observation**

The fixed specimens were decalcified in an acid decalcifying solution and were dehydrated in a series of ethanol with concentration ascending from 70% to 100%. The specimens were then paraffinized, bisected, and finally embedded in paraffin blocks ready for histological sectioning. Five-micrometer-thick coronal sections were obtained from the central region of the circular defects using a semi-automated rotary microtome (Leica RM2245, Leica Biosystems, Germany) and were then moved to coated glass slides. The slides with tissue sections were de-paraffinized and hydrated through a series of xylene and graded ethanol and were finally stained with hematoxylin & eosin (H&E) for visualization under an optical light microscope.

### 5.17. Statistical analysis

A one-way analysis of variance (ANOVA) was performed to compare the different groups, and the results were considered to be statistically significant at  $p < 0.05$  (\*) or  $p < 0.01$  (\*\*) with the differences between groups compared using Tukey's test.

**Acknowledgment:** This study was supported by a grant from the Priority Research Centers Program (2009-0093829), National Research Foundation, South Korea.

**Figure caption**

**Fig. 1.** Properties of mBGn added to CPC formulations; (a) TEM image and EDS atomic composition in the inset; (b) XRD patterns collected after soaking mBGn in SBF for different time periods, revealing the characteristic apatite peaks.

**Table 1.** Characteristics of the mBGn and  $\alpha$ -TCP used for CPC powder compositions, including mesoporosity and  $\zeta$ -potential.

**Fig. 2.** Characteristics of the as-cemented samples; (a) SEM micrographs; (b) XRD phase pattern, revealing all samples had  $\alpha$ -TCP peaks as the main phase; Symbols “○”, “●” and “❖” corresponding to  $\alpha$ -TCP (JCPDS Card No. 09-348),  $\beta$ -TCP (JCPDS Card No. 09-169) and HA (JCPDS Card No. 09-432), respectively (c) FT-IR analyses showing Si-O and Si-O-Si bands increasing in intensity with an increase in mBGn contents.

**Fig. 3.** Setting time measurement of the cements at varying L/P ratios (0.55, 0.65, and 0.75 ml/g) with respect to the mBGn content. The setting reaction gradually accelerated with an increase in the mBGn content.

**Fig. 4.** Change in the cements after 7 days of soaking in SBF, revealing a substantial degree of apatite formation. Symbol “○” corresponding to HA (JCPDS Card No. 09-432); (a–d) representative SEM images shown for 0% (a, b) and 10% mBGn (c,d) at different magnifications; (e) XRD phase change; (f) FT-IR spectra.

**Fig. 5.** (a) Surface area and (b) porosity changes of the cements with respect to an increase in the mBGn content. The samples prepared both with or without immersion in SBF were measured.

**Fig. 6.** Compressive strength of the cements. The SBF-immersed samples had higher values than the untreated ones, and the addition of mBGn improved the mechanical strength.

**Fig. 7.** Injectability study of the cements. (a–c) Representative injectability curves for cements incorporated with 0, 5, and 10% mBGn (L/P = 0.45 ml/g) obtained from a syringe with a 2-mm diameter under a compression rate of 15 mm/min and a maximum applied injection force of 150 N. (d) Injectability percentage measured for different cement compositions.

**Fig. 8.** Wash-out and consistency tests of the cements. (a) Weight changes recorded after the wash-out test, and the sample photos are included as insets in the graph; (b) Spread diameters measured after the consistency test with sample photos. Addition of mBGn enhanced both resistance to wash-out and consistency.

**Fig. 9.** Ion release from the samples; (a) pure mBGn; (b) cement with 0% mBGn, and (c) cement with 10% mBGn; Ca, P, and Si ions measured after soaking in Tris-Buffer (pH 7.4) at 37 °C for different time periods.

**Fig. 10.** pH variations measured during immersion of the cement samples in PBS at 37 °C. The mBGn addition increased the pH significantly. Inset image enlarged the initial response period.

**Fig. 11.** Protein (Cyto c) adsorption test showing mBGn addition enhanced the protein adsorption capacity of the cements.

**Fig. 12.** In vivo biocompatibility of 0% and 10% mBGn cements in rat subcutaneous tissue at 4 week post-operation. H&E and MT stains. C: cement. Scale bar: 350  $\mu\text{m}$ .

**Fig. 13.** In vivo study of cement samples in rat calvarium for 6 weeks. Block type cements implanted and the histological images showing bone formation at the interface of cement-tissue. (a) 0% and (b) 10% mBGn cement at different magnifications. C: cement; HB: host bone; NB: new bone. Scale bar: 350  $\mu\text{m}$ .

## References

- 1 A. Sugawara, K. Asaoka and S. J. Ding, *J. Mater. Chem. B*, 2013, **1**, 1081-1089.
- 2 M. Bohner, *Eur. Cell. Mater.*, 2010, **20**, 1-12.
- 3 N. Suhm and A. Gisepp, *J. Ortho. Trau.*, 2008, **22**, S121-125.
- 4 D. P. Link, J. van den Dolder, J. J. van den Beucken, J. G. Wolke, A. G. Mikos and J. A. Jansen, *Biomater.*, 2008, **29**, 675-682.
- 5 M. Bohner, U. Gbureck and J. E. Barralet, *Biomater.*, 2005, **26**, 6423-6429.
- 6 M. P. Ginebra, T. Traykova and J. A. Planell, *J. Cont. Rel.*, 2006, **113**, 102-110.
- 7 S. Dorozhkin, *J. Func. Biomater.*, 2013, **4**, 209-311.
- 8 S.Y. Kim and S.H. Jeon *J. Indust. Eng. Chem.* 2012, **18**,128-36.
- 9 C. Durucan and P. W. Brown, *J. Mater. Sci: Mater. Med.*, 2000, **11**, 365-371.
- 10 M. Bohner, *Biomater.*, 2004, **25**, 741-749.
- 11 M. Espanol, R. A. Perez, E. B. Montufar, C. Marichal, A. Sacco and M. P. Ginebra, *Acta Biomater.*, 2009, **5**, 2752-2762.
- 12 S. A. Oh, G. S. Lee, J. H. Park and H. W. Kim, *J. Mater. Sci: Mater. Med.*, 2010, **21**, 3019-3027.
- 13 R. G. Carrodeguas and S. De Aza, *Acta Biomater.*, 2011, **7**, 3536-3546.
- 14 H. Guo, J. Su, J. Wei, H. Kong and C. Liu, *Acta Biomater.*, 2009, **5**, 268-278.
- 15 I. Rajzer, O. Castano, E. Engel and J. A. Planell, *J. Mater. Sci: Mater. Med.*, 2010, **21**, 2049-2056.
- 16 F. Wu, J. Wei, H. Guo, F. Chen, H. Hong and C. Liu, *Acta Biomater.*, 2008, **4**, 1873-1884.
- 17 C. Canal and M. P. Ginebra, *J. Mech. Behav. Biomed. Mater.*, 2011, **4**, 1658-1671.
- 18 R. Krüger and J. Groll, *Biomater.*, 2012, **33**, 5887-5900.
- 19 R. P. Félix Lanao, S. C. G. Leeuwenburgh, J. G. C. Wolke and J. A. Jansen, *Biomater.*, 2011, **32**, 8839-8847.
- 20 A. C. M. Renno, F. C. J. van de Watering, M. R. Nejadnik, M. C. Crovace, E. D. Zanotto, J. G. C. Wolke, J. A. Jansen and J. J. J. P. van den Beucken, *Acta Biomater.*, 2013, **9**, 5728-5739.
- 21 C. Bao, W. Chen, M. D. Weir, W. Thein-Han and H. H. K. Xu, *Acta Biomater.*, 2011, **7**, 4037-4044.
- 22 M. Schumacher, A. Lode, A. Helth and M. Gelinsky, *Acta Biomater.*, 2013, **9**, 9547-9557.
- 23 E. M. Ooms, J. G. C. Wolke, M. T. van de Heuvel, B. Jeschke and J. A. Jansen, *Biomater.*, 2003, **24**, 989-1000.

- 24 D. Apelt, F. Theiss, A. O. El-Warrak, K. Ziinszky, R. Bettschart-Wolfisberger, M. Bohner, S. Matter, J. A. Auer and B. von Rechenberg, *Biomater.*, 2004, **25**, 1439-1451.
- 25 E. S. Sanzana, M. Navarro, F. Macule, S. Suso, J. A. Planell and M. P. Ginebra, *Acta Biomater.*, 2008, **4**, 1924-1933.
- 26 M. Ventura, Y. Sun, S. Cremers, P. Borm, Z. T. Birgani, P. Habibovic, A. Heerschap, P. M. van der Kraan, J. A. Jansen and X. F. Walboomers, *Biomater.*, 2014, **35**, 2227-2233.
- 27 I. M. Martínez, P. Velásquez, L. Meseguer-Olmo, A. Bernabeu-Esclapez and P. N. De Aza, *Mater. Sci. Eng: C*, 2012, **32**, 878-886.
- 28 M. P. Ginebra, C. Canal, M. Espanol, D. Pastorino and E. B. Montufar, *Adv. Drug Deliv. Rev.*, 2012, **64**, 1090-1110.
- 29 C. Liu, C. W. Chen, P. Ducheyne, *Biomed. Mater.*, 2008, **3**, 034111.
- 30 M. D. Vlad, L.J. del Valle, M. Barraco, R. Torres, J. Lopez, E. Fernandez, *Spine*, 2008, **33**, 2290-2298.
- 31 Y. Zuo, F. Yang, J. G. Wolke, Y. Li and J. A. Jansen, *Acta Biomater.*, 2010, **6**, 1238-1247.
- 32 S. Borhan, S. Hesarakhi and S. Ahmadzadeh-Asl, *J. Mater. Sci: Mater. Med.*, 2010, **21**, 3171-3181.
- 33 N. Nezafati, F. Moztarzadeh, S. Hesarakhi and M. Mozafari, *Ceramics Int.*, 2011, **37**, 927-934.
- 34 H. Guo , J. Wei , W. Song , S. Zhang , Y. Yan , C. Liu , T. Xiao , *Int. J. Nanomed.*, 2012, **7**, 3613-24.
- 35 S. Hesarakhi, M. Alizadeh, S. Borhan and M. Pourbaghi-Masouleh, *J. Biomed. Mater. Res. B, App. Biomater.*, 2012, **100**, 1627-1635.
- 36 L. Yu, Y. Li, K. Zhao, Y. Tang, Z. Cheng, J. Chen, Y. Zang, J. Wu, L. Kong, S. Liu, W. Lei and Z. Wu, *PLoS ONE*, 2013, **8**, e62570.
- 37 N. Nezafati, F. Moztarzadeh, S. Hesarakhi, Z. Moztarzadeh and M. Mozafari, *Ceramics Int.*, 2013, **39**, 289-297.
- 38 F. C. van de Watering, J. J. van den Beucken, X. F. Walboomers and J. A. Jansen, *Clin. Oral Imp. Res.*, 2012, **23**, 151-159.
- 39 A. Sadiasa, S. K. Sarkar, R. A. Franco, Y. K. Min and B. T. Lee, *J. Biomater App.*, 2014, **28**, 739-756.
- 40 H. Zhou, T. J. Luchini, A. K. Agarwal, V. K. Goel and S. B. Bhaduri, *J. Biomed. Mater. Res. B, App. Biomater.*, 2014, **102**, 1620-1626.
- 41 S. Takagi, L. C. Chow, S. Hirayama and F. C. Eichmiller, *Dental Mater.*, 2003, **19**, 797-804.

- 42 A. Bigi, B. Bracci and S. Panzavolta, *Biomater.*, 2004, **25**, 2893-2899.
- 43 R. A. Perez and M. P. Ginebra, *J. Mater. Sci: Mater. Med.*, 2013, **24**, 381-393.
- 44 G. S. Lee, J. H. Park, U. S. Shin and H.-W. Kim, *Acta Biomater.*, 2011, **7**, 3178-3186.
- 45 G. S. Lee, J. H. Park, J. E. Won, U. Shin and H.-W. Kim, *J. Mater. Sci: Mater. Med.*, 2011, **22**, 1257-1268.
- 46 RA Perez , HW Kim , MP Ginebra, *J. Tissue Eng.* 2012, **3** 2041731412439555.
- 47 R. A. Pérez, J.-E. Won, J. C. Knowles and H.-W. Kim, *Adv. Drug Deliv. Rev.*, 2013, **65**, 471-496.
- 48 D. P. Link, J. van den Dolder, W. J. F. M. Jurgens, J. G. C. Wolke and J. A. Jansen, *Biomater.*, 2006, **27**, 4941-4947.
- 49 P. Q. Ruhe, E. L. Hedberg-Dirk, N. T. Padron, P. H. Spauwen, J. A. Jansen and A. G. Mikos, *Tissue Eng.*, 2006, **12**, 789-800.
- 50 X. Wang, J. Ye, Y. Wang and L. Chen, *J. Am. Cer. Soc.*, 2007, **90**, 962-964.
- 51 K. K. Chew, K. L. Low, S. H. Sharif Zein, D. S. McPhail, L. C. Gerhardt, J. A. Roether and A. R. Boccaccini, *J. Mech. Behav. Biomed. Mater.*, 2011, **4**, 331-339.
- 52 S. I. Roohani-Esfahani, S. Nouri-Khorasani, Z. F. Lu, R. C. Appleyard and H. Zreiqat, *Acta Biomater.*, 2011, **7**, 1307-1318.
- 53 J. J. Kim, S. H. Bang, A. El-Fiqi and H. W. Kim, *Mater. Chem. Phys.*, 2014, **143**, 1092-1101.
- 54 S. I. Roohani-Esfahani, S. Nouri-Khorasani, Z. F. Lu, M. H. Fathi, M. Razavi, R. C. Appleyard and H. Zreiqat, *Mater. Sci. Eng: C*, 2012, **32**, 830-839.
- 55 K. D. Patel, A. El-Fiqi, H.-Y. Lee, R. K. Singh, D.-A. Kim, H.-H. Lee and H.-W. Kim, *J. Mater. Chem.*, 2012, **22**, 24945-24956.
- 56 G. M. Luz and J. F. Mano, *Biomed. Mater.*, 2012, **7**, 054104.
- 57 S. K. Misra, D. Mohn, T. J. Brunner, W. J. Stark, S. E. Philip, I. Roy, V. Salih, J. C. Knowles and A. R. Boccaccini, *Biomater.*, 2008, **29**, 1750-1761.
- 58 B. Marelli, C. E. Ghezzi, D. Mohn, W. J. Stark, J. E. Barralet, A. R. Boccaccini and S. N. Nazhat, *Biomater.*, 2011, **32**, 8915-8926.
- 59 A. El-Fiqi, J. H. Lee, E. J. Lee and H. W. Kim, *Acta Biomater.*, 2013, **9**, 9508-9521.
- 60 M. Vollenweider, T. J. Brunner, S. Knecht, R. N. Grass, M. Zehnder, T. Imfeld and W. J. Stark, *Acta Biomater.*, 2007, **3**, 936-943.

- 61 A. El-Fiqi, T. H. Kim, M. Kim, M. Eltohamy, J. E. Won, E. J. Lee and H. W. Kim, *Nanoscale*, 2012, **4**, 7475-7488.
- 62 ASTM standard C266-08 "Standard Test Method for Time of Setting of Hydraulic Cement Paste by Gillmore Needles". American Society for Testing and Materials (ASTM); West Conshohocken, USA 2008; doi:10.1520/C0266-08.
- 63 M. P. Ginebra, J. A. Delgado, I. Harr, A. Almirall, S. Del Valle and J. A. Planell, *J. Biomed. Mater. Res. A*, 2007, **80**, 351-361.
- 64 M. P. Ginebra, A. Rilliard, E. Fernandez, C. Elvira, J. San Roman and J. A. Planell, *J. Biomed. Mater. Res.*, 2001, **57**, 113-118.
- 65 Y. Miyamoto, K. Ishikawa, M. Takechi, T. Toh, T. Yuasa, M. Nagayama and K. Suzuki, *Biomater.*, 1998, **19**, 707-715.
- 66 K. Ishikawa, S. Matsuya, M. Nakagawa, K. Udoh and K. Suzuki, *J. Mater. Sci: Mater. Med.*, 2004, **15**, 13-17.
- 67 K. Ishikawa, Y. Miyamoto, M. Takechi, T. Toh, M. Kon, M. Nagayama and K. Asaoka, *J. Biomed. Mater. Res.*, 1997, **36**, 393-399.
- 68 M. Takechi, Y. Miyamoto, K. Ishikawa, M. Nagayama, M. Kon, K. Asaoka and K. Suzuki, *J. Biomed. Mater. Res.*, 1998, **39**, 308-316.
- 69 G. Gupta, S. Kirakodu and A. El-Ghannam, *J. Biomed. Mater. Res. A*, 2007, **80A**, 486-496.
- 70 E. Boanini, M. Gazzano and A. Bigi, *Acta Biomater.*, 2010, **6**, 1882-1894.
- 71 G. Mestres, C. Le Van and M.-P. Ginebra, *Acta Biomater.*, 2012, **8**, 1169-1179.
- 72 S. Bose, G. Fielding, S. Tarafder and A. Bandyopadhyay, *Trends in Biotech.*, 2013, **31**, 594-605.
- 73 P. Han, C. Wu and Y. Xiao, *Biomater. Sci.*, 2013, **1**, 379-392.
- 74 J. H. Jang, Y. Ku, C. P. Chung and S. J. Heo, *Biotech. Lett.*, 2002, **24**, 1659-1663.
- 75 B.G. Keselowsky, D.M. Collard and A.J. Garcia, *J. Biomed. Mater. Res. A*, 2003, **66**, 247-259.
- 76 K. Wang, C. Zhou, Y. Hong and X. Zhang, *Interface Focus*, 2012.
- 77 S. Samavedi, A. R. Whittington and A. S. Goldstein, *Acta Biomater.*, 2013, **9**, 8037-8045.
- 78 M. Bohner and G. Baroud, *Biomater.*, 2005, **26**, 1553-1563.
- 79 SV. Dorozhkin, *Int. J. Mater. Chem.*, 2011, **1**, 1-48.

- 80 A. C. Renno, M.R. Nejadnik, F. C. van de Watering, M. C. Crovace, E. D. Zanotto, J.P. Hoefnagels, J. G. Wolke, J. A. Jansen and J. J. van den Beucken, *J. Biomed. Mater. Res. A*, 2013, **101**, 2365-2373.
- 81 R. P. Felix Lanao, K. Sariibrahimoglu, H. Wang, J. G. Wolke, J. A. Jansen and S. C. Leeuwenburgh, *Tissue Eng. A*, 2014, **20**, 378-388.
- 82 C. Wu, J. Chang and W. Fan, *Journal of Materials Chemistry*, 2012, **22**, 16801-16809.
- 83 C. Wu, W. Fan and J. Chang, *Journal of Materials Chemistry B*, 2013, **1**, 2710-2718.
- 84 X. Yan, C. Yu, X. Zhou, J. Tang and D. Zhao, *Angewandte Chemie (International ed. in English)*, 2004, **43**, 5980-5984.
- 85 C. Wu, Y. Ramaswamy, Y. Zhu, R. Zheng, R. Appleyard, A. Howard and H. Zreiqat, *Biomaterials*, 2009, **30**, 2199-2208.
- 86 C. Wu, Y. Zhang, Y. Zhou, W. Fan and Y. Xiao, *Acta Biomater*, 2011, **7**, 2229-2236.
- 87 P. Horcajada, A. Rámila, K. Boulahya, J. González-Calbet and M. Vallet-Regí, *Solid State Sciences*, 2004, **6**, 1295-1300.
- 88 A. López-Noriega, D. Arcos, I. Izquierdo-Barba, Y. Sakamoto, O. Terasaki and M. Vallet-Regí, *Chemistry of Materials*, 2006, **18**, 3137-3144.
- 89 J. Sun, Y. Li, L. Li, W. Zhao, L. Li, J. Gao, M. Ruan and J. Shi, *Journal of Non-Crystalline Solids*, 2008, **354**, 3799-3805.
- 90 W. Xia and J. Chang, *Journal of Controlled Release*, 2006, **110**, 522-530.
- 91 Y. Hong, X. Chen, X. Jing, H. Fan, B. Guo, Z. Gu and X. Zhang, *Advanced materials*, 2010, **22**, 754-758.
- 92 C. Wu, Y. Zhou, M. Xu, P. Han, L. Chen, J. Chang and Y. Xiao, *Biomaterials*, 2013, **34**, 422-433.

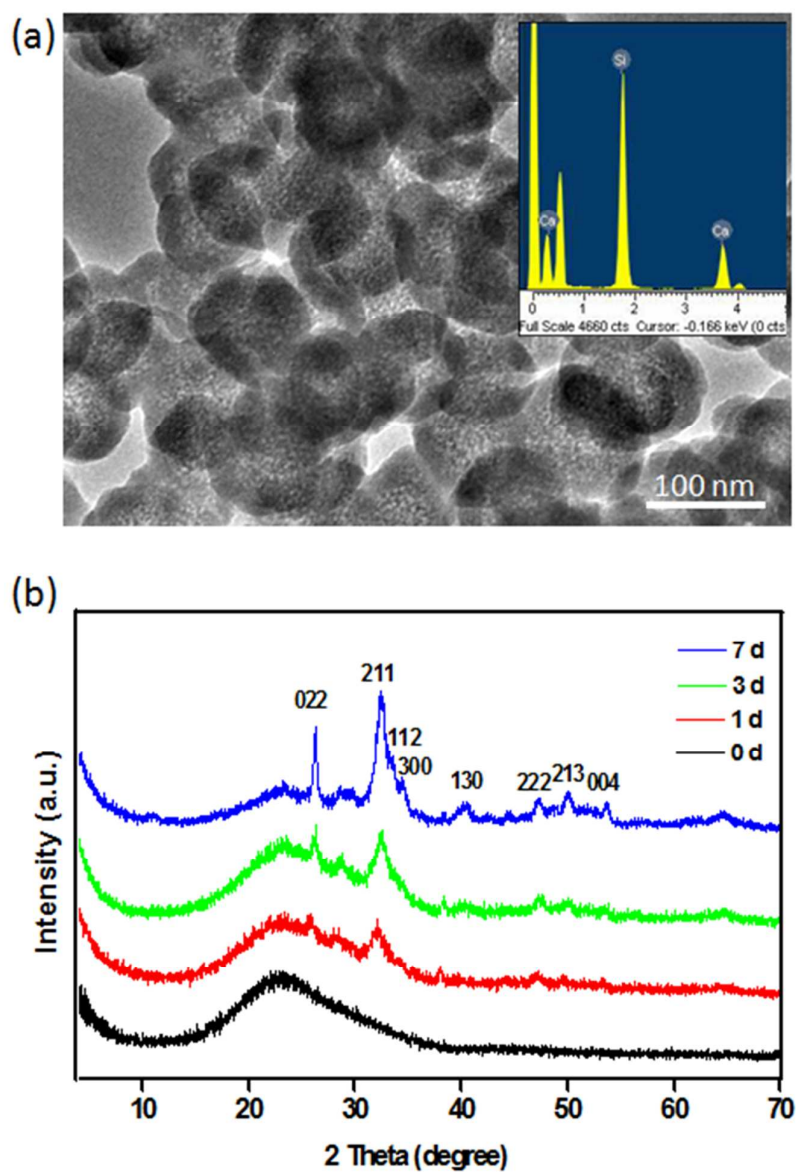


**Fig. 1.** Properties of mBGn added to CPC formulations; (a) TEM image and EDS atomic composition in the inset; (b) XRD patterns collected after soaking mBGn in SBF for different time periods, revealing the characteristic apatite peaks.

**Table 1.** Characteristics of the mBGn and  $\alpha$ -TCP used for CPC powder compositions, including mesoporosity and  $\zeta$ -potential.

Parameter	mBGn	$\alpha$ -TCP
Particle size	80 - 90 nm	5 - 10 $\mu$ m
$S_{\text{BET}}$ ( $\text{m}^2/\text{g}$ )	$54.0 \pm 0.928$	$0.864 \pm 0.013$
Pore $\varnothing$ (nm)	4.9	-
Pore Vol. ( $\text{cm}^3/\text{g}$ )	0.133	-
Zeta potential (mV)	$-29 \pm 1.34$	$-15.1 \pm 1.1$

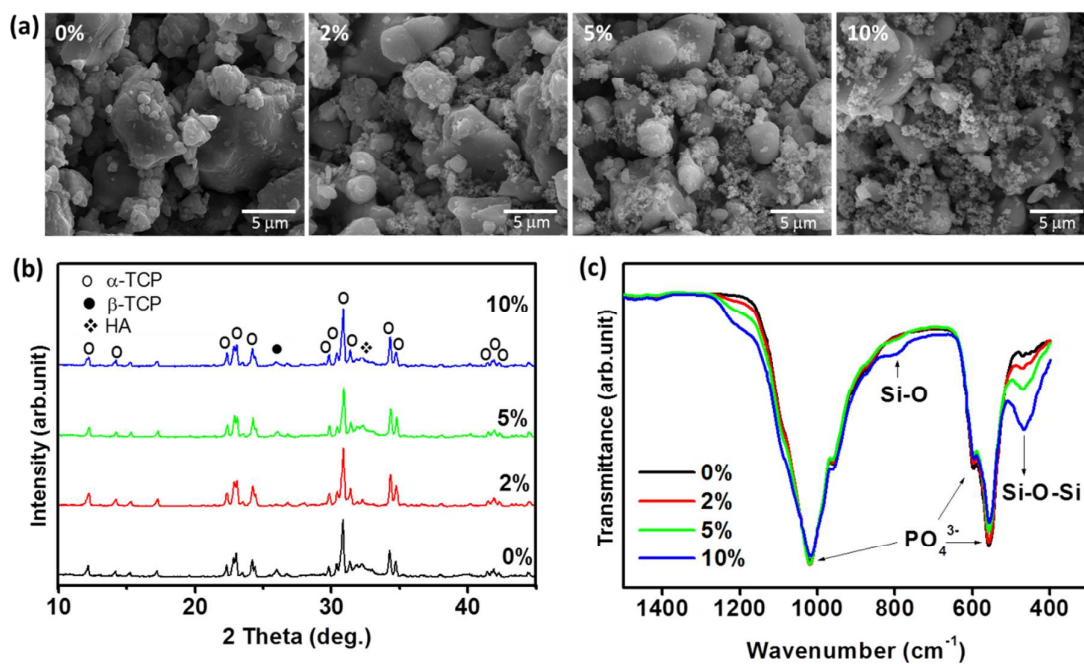


**Fig. 2.** Characteristics of the as-cemented samples; (a) SEM micrograph with EDS profiles in the insets; (b) XRD phase development, revealing all samples had similar  $\alpha$ -TCP peaks; (c) FT-IR analyses showing Si-O-Si and Si-O bands increasing in intensity with an increase in mBGN contents.

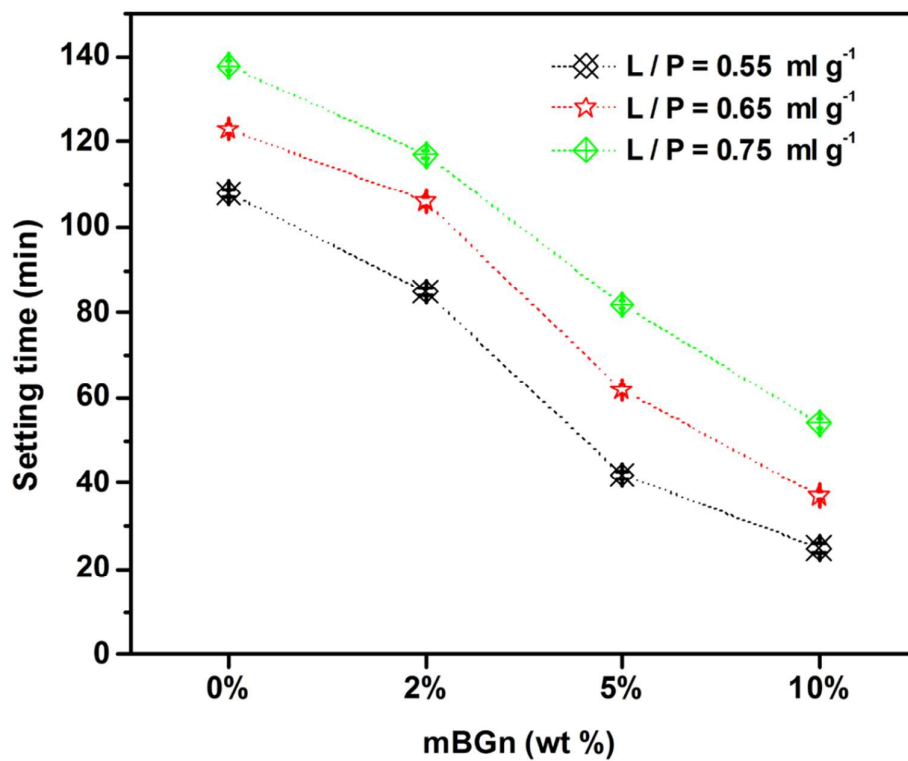


**Fig. 3.** Setting time measurement of the cements at varying L/P ratios (0.55, 0.65, and 0.75 ml/g) with respect to the mBGn content. The setting reaction gradually accelerated with an increase in the mBGn content.

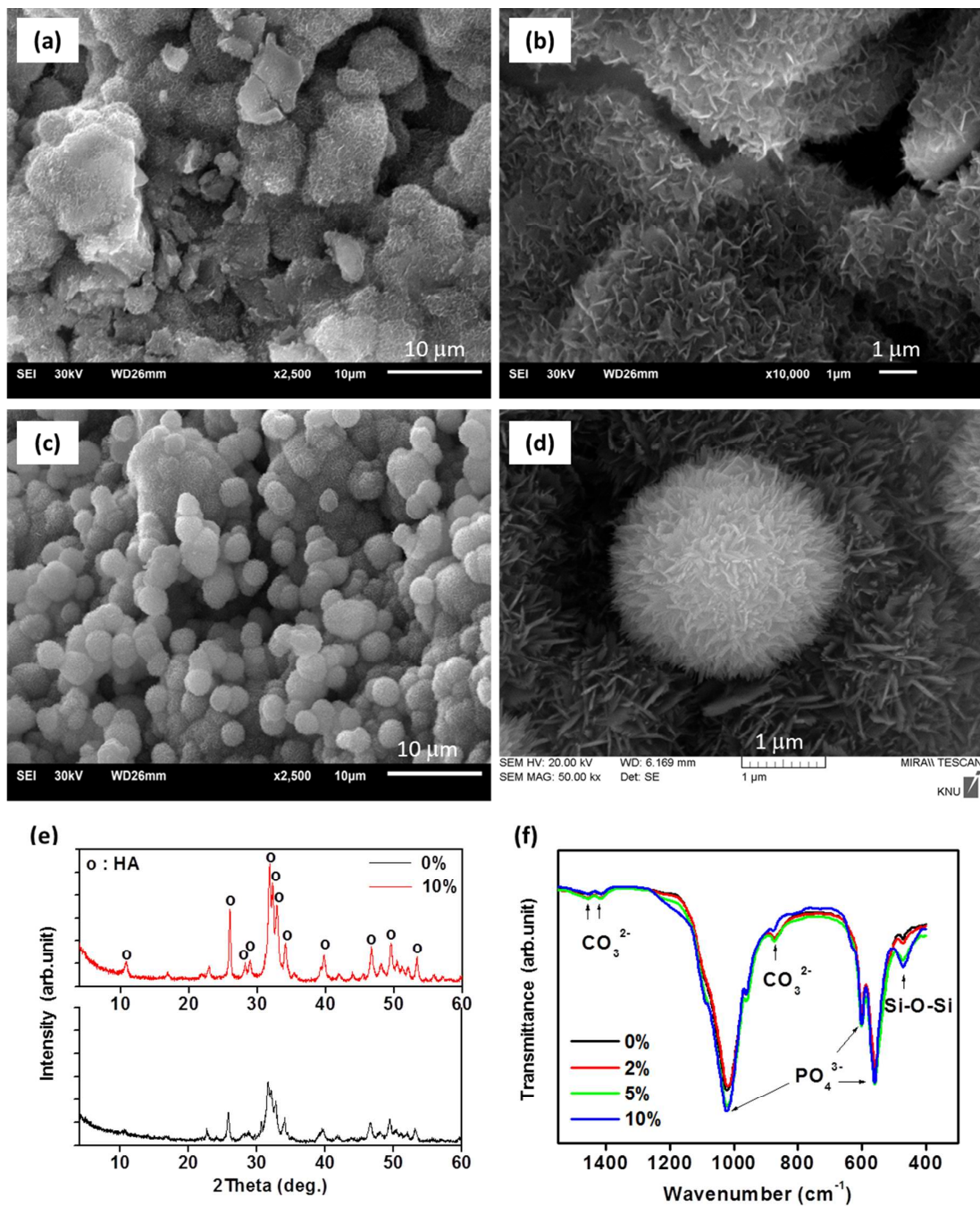


**Fig. 4.** Change in the cements after 7 days of soaking in SBF, revealing a substantial degree of apatite formation; (a–d) representative SEM images shown for 0% (a, b) and 10% mBGn (c,d) at different magnifications; (e) XRD phase change; (f) FT-IR spectra.

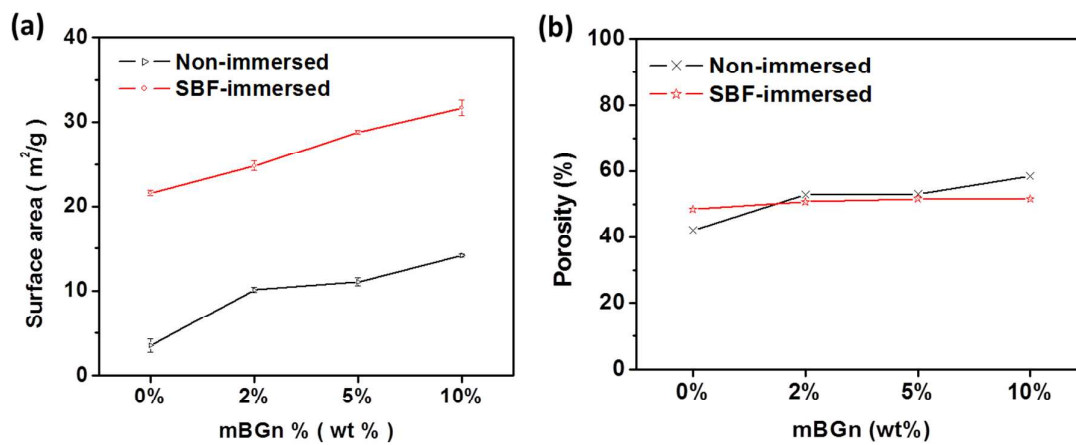


**Fig. 5.** (a) Surface area and (b) porosity changes of the cements with respect to an increase in the mBGn content. The samples prepared both with or without immersion in SBF were measured.

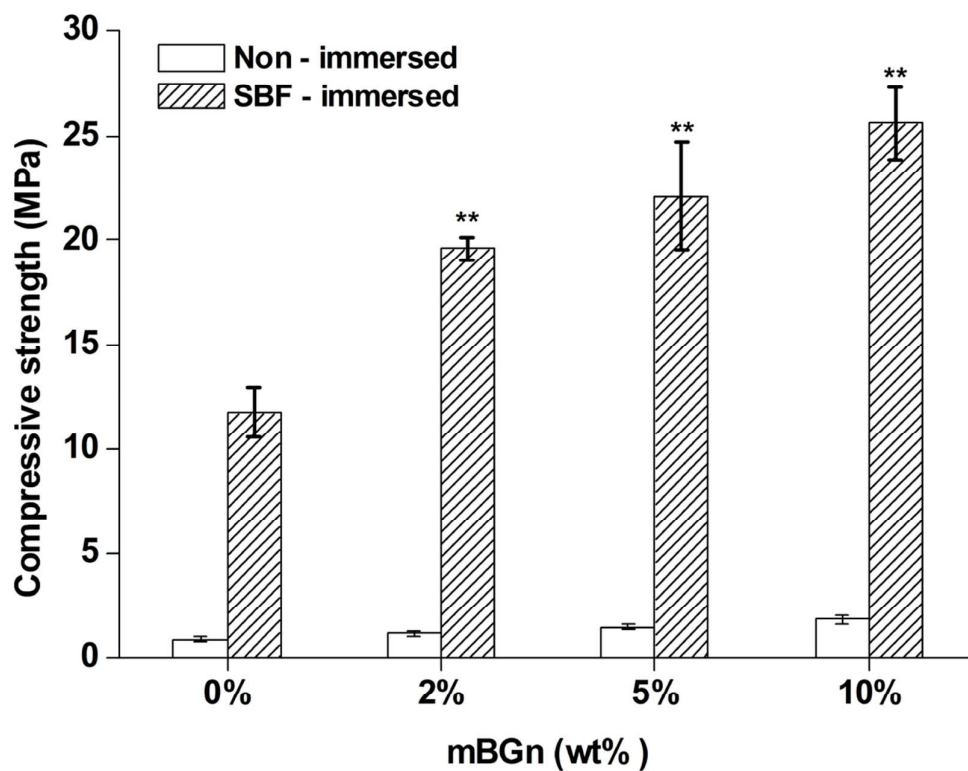


**Fig. 6.** Compressive strength of the cements. The SBF-immersed samples had higher values than the untreated ones, and the addition of mBGn improved the mechanical strength.

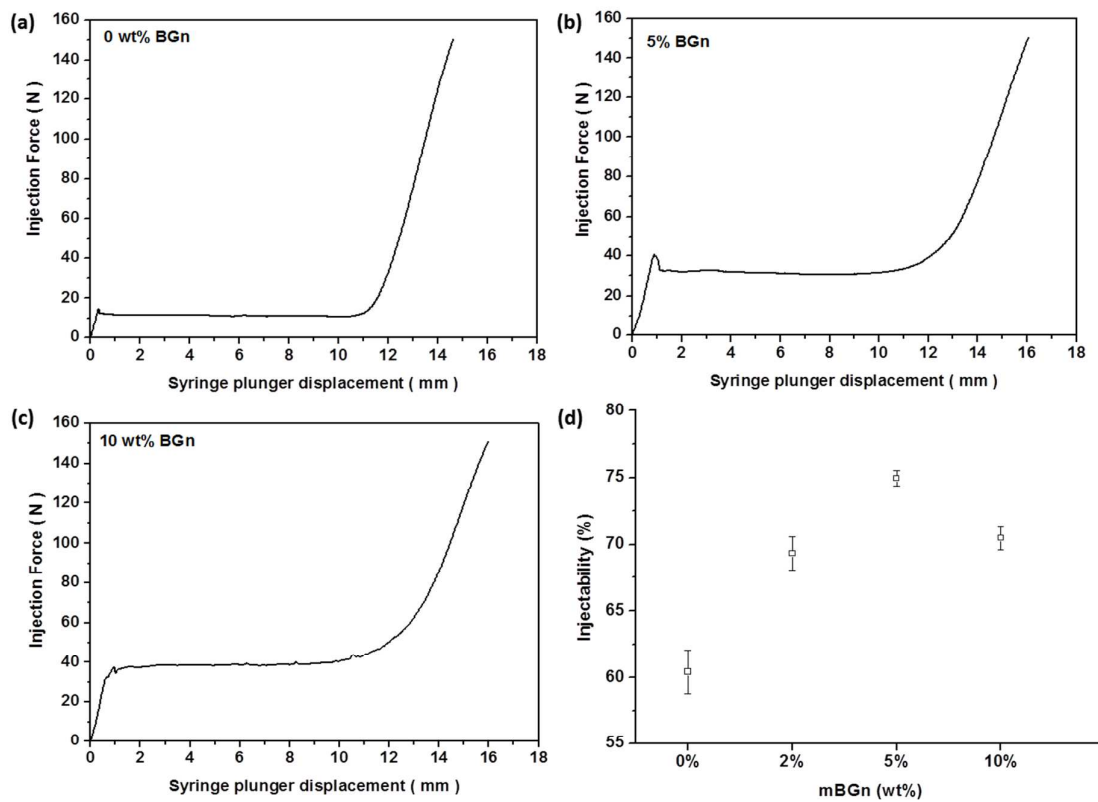


**Fig. 7.** Injectability study of the cements. (a–c) Representative injectability curves for cements incorporated with 0, 5, and 10% mBGn ( $L/P = 0.45$  ml/g) obtained from a syringe with a 2-mm diameter under a compression rate of 15 mm/min and a maximum applied injection force of 150 N. (d) Injectability percentage measured for different cement compositions.

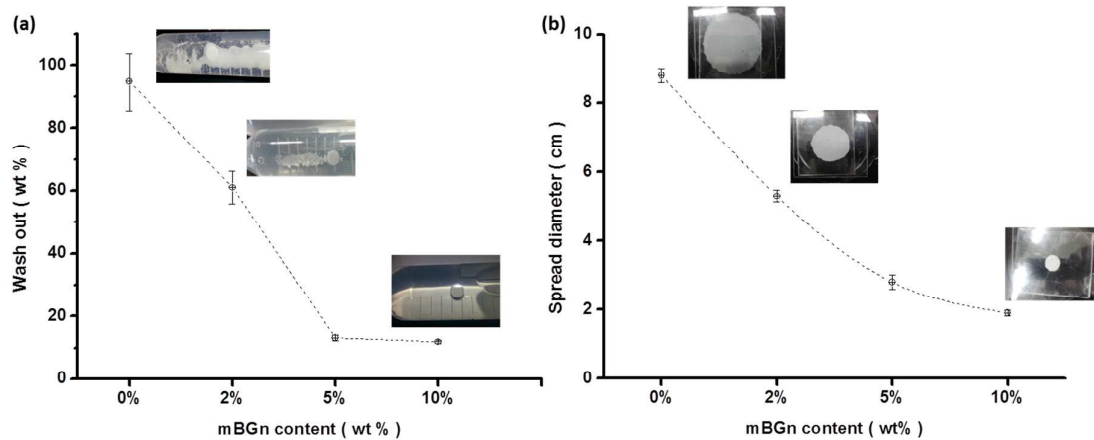


**Fig. 8.** Wash-out and consistency tests of the cements. (a) Weight changes recorded after the wash-out test, and the sample photos are included as insets in the graph; (b) Spread diameters measured after the consistency test with sample photos. Addition of mBGn enhanced both resistance to wash-out and consistency.

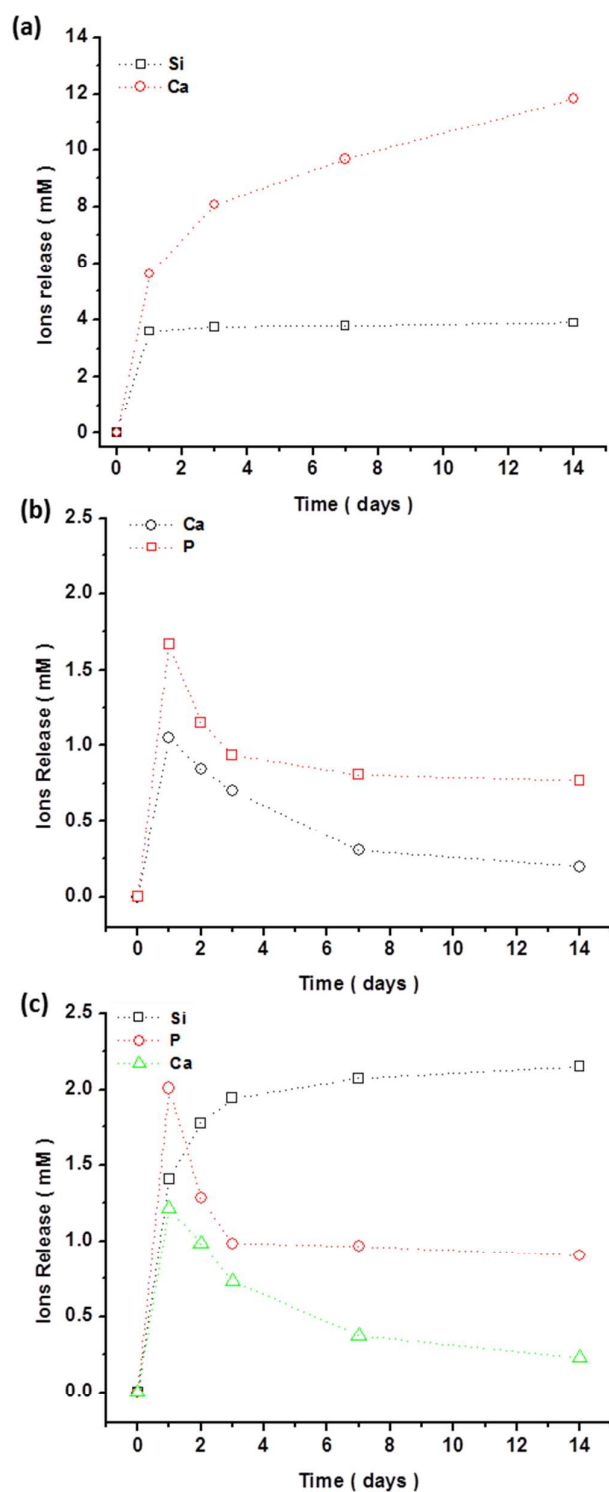


**Fig. 9.** Ion release from the samples; (a) pure mBGn; (b) cement with 0% mBGn, and (c) cement with 10% mBGn; Ca, P, and Si ions measured after soaking in Tris-Buffer (pH 7.4) at 37 °C for different time periods.

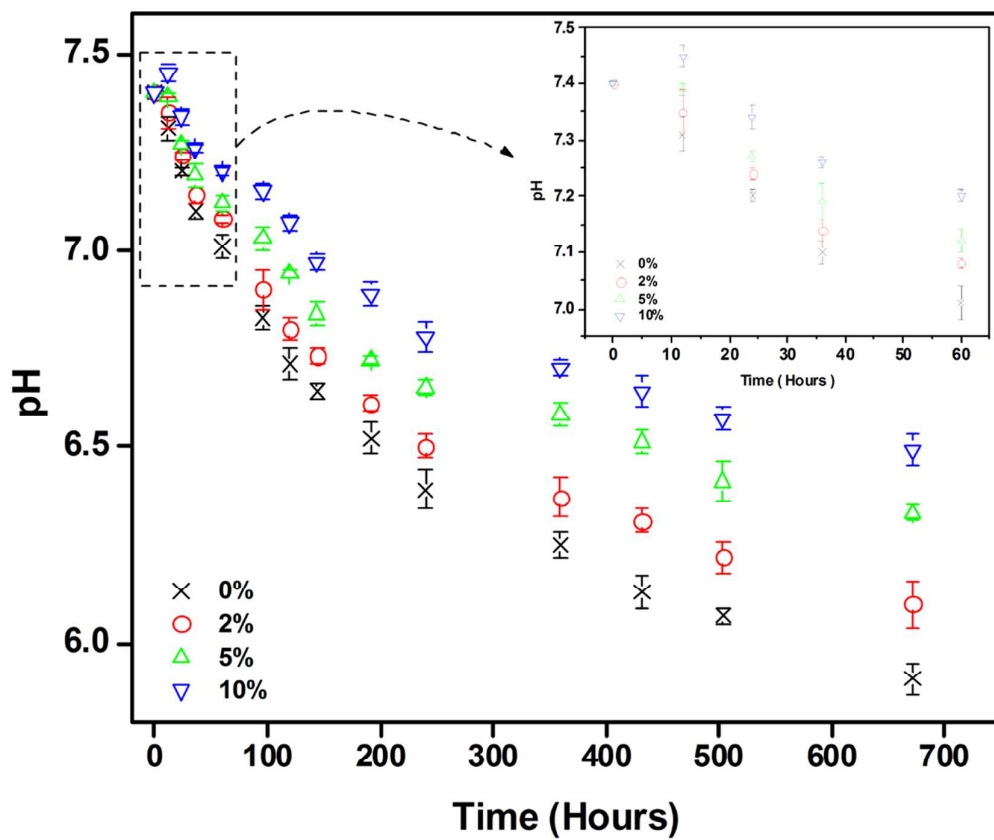


**Fig. 10.** pH variations measured during immersion of the cement samples in PBS at 37 °C. The mBGn addition increased the pH significantly. Inset image enlarged the initial response period.

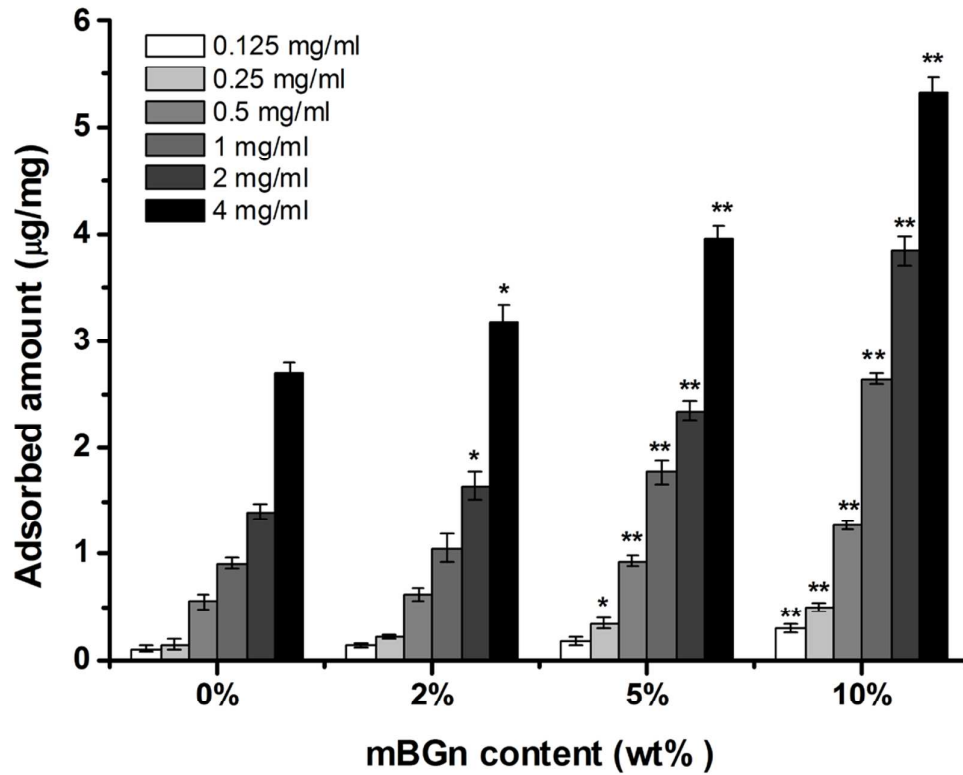


**Fig. 11.** Protein (cyto c) adsorption test showing mBGn addition enhanced the protein adsorption capacity of the cements.

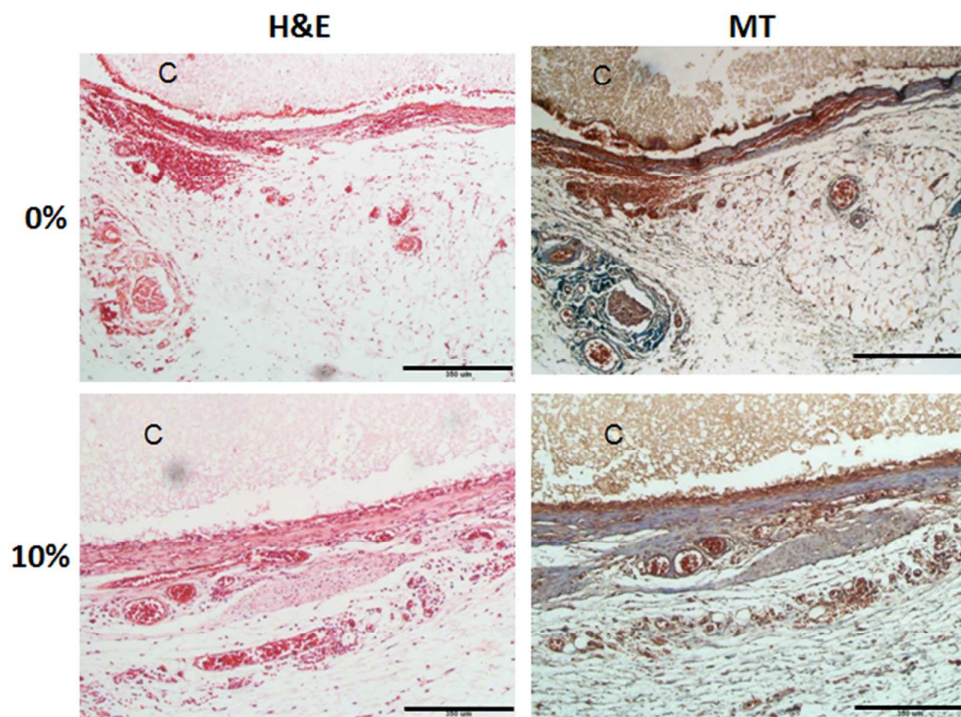


**Fig. 12.** In vivo compatibility of 0% and 10% mBGn cements in rat subcutaneous tissue at 4 week post-operation. H&E and MT stains. C: cement. Scale bar: 350  $\mu$ m.

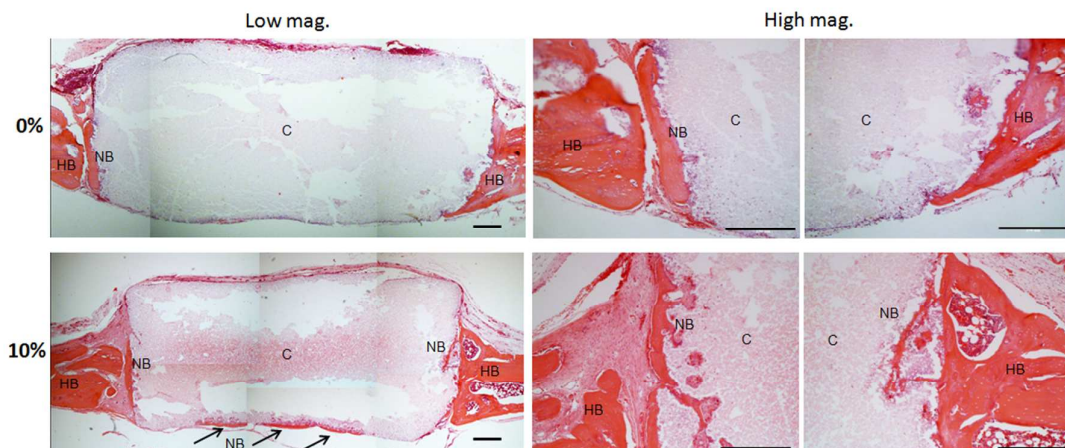


**Fig. 13.** In vivo study of cement samples in rat calvarium for 6 weeks. Block type cements implanted and the histological images showing bone formation at the interface of cement-tissue. (a) 0% and (b) 10% mBGn cement at different magnifications. C: cement; HB: host bone; NB: new bone. Scale bar: 350  $\mu\text{m}$ .

## Graphical abstract

